journal

J. Am. Ceram. Soc., 97 [1] 316–325 (2014)
DOI: 10.1111/jace.12665

In Situ Observation of the Dissolution of SiO_2 Particles in $CaO–Al_2O_3–SiO_2$ Slags and Mathematical Analysis of its Dissolution Pattern

Stefan Feichtinger,[‡] Susanne K. Michelic,[‡] Youn-Bae Kang,[§,†] and Christian Bernhard[‡]

[‡]Chair of Ferrous Metallurgy, Montanuniversitaet Leoben, Leoben A-8700, Austria

[§]Graduate Institute of Ferrous Technology, Pohang University of Science and Technology (POSTECH), Pohang, Kyungbuk 790-784, Korea

The dissolution of amorphous SiO_2 particles in $CaO–Al_2O_3–SiO_2$ slags was investigated at 1450°C by high-temperature confocal scanning laser microscopy (HT-CSLM) and thermodynamic/kinetic analyses. The SiO_2 particles used in this experimental study had a spherical form so that any rotation of the particle did not cause errors in the determination of the particle size during the dissolution. Moreover, a wide composition range of the slag could be chosen without forming any solid reaction layer which could distort the evaluation of the dissolution mechanism. The evolution of the diameter of the spherical SiO_2 particle was measured by image analysis of pictures obtained from the HT-CSLM. It was found that the dissolution curve of the SiO_2 particle (size as a function of time) exhibited either a parabolic-like curve or an S-shaped curve depending on the slag composition. The patterns were compared with a well-known shrinking core model (SCM), and it was shown that the SCM could not represent the dissolution behavior of the SiO_2 particle observed in this study. It was experimentally found that the shape of the dissolution curves varies as a function of the slag composition. The curve exhibited a parabolic-like shape for low SiO_2-containing slags and changed to an S-type shape with increasing SiO_2 concentration in the slag. To elucidate the dissolution mechanism, a model based on approximations for the diffusion near the particle was proposed by modifying the previously available model [M. J. Whelan, *Met. Sci. J.*, 3, 95–97 (1969)]. From the experimental data and the model calculations, the viscosity of the slag was shown to be the major factor affecting both dissolution rate and mechanism. Effective binary diffusion coefficients were estimated using the model and experimental data. Those were shown to be in the range of literature data.

I. Introduction

Steel wires are high-strength steel products which require high cleanliness. Demanding steel wire products include for example tire cord, valve spring, and saw wire. Nonmetallic inclusions are known to be the main reason for wire breakage during both production and application.[1,2] Countermeasures to avoid nondeformable inclusions causing breakage have mainly targeted at alumina inclusions in the past. In particular, replacing ladle refractories with nonalumina type materials, using ferroalloys of low Al content, Si deoxidation, and low alumina ladle slags helped to reduce the wire breakage rate.[2,3] However, low alumina $CaO–Al_2O_3–SiO_2$ (CAS) slags and a relatively high silicon content in the steel then caused the formation of SiO_2 inclusions. The thermodynamics of the mentioned slags were studied extensively by various authors.[4–8] It was shown that crystallized SiO_2 inclusions can cause wire breakage as they are nondeformable.[9] The origins of SiO_2 inclusions found in final wire products are categorized into two types: SiO_2 inclusions might either form as a deoxidation product or precipitate during casting. While the latter is out of scope in this study, the former should be removed as much as possible during the refining process. It requires a relevant investigation about the dissolution of SiO_2 inclusions in refining slags. Design of top slags which leads to fast dissolution of SiO_2 inclusions is thus necessary to be investigated. As the formation of nonmetallic inclusions cannot be avoided completely, efficient removal of nonmetallic inclusions by slags needs to be ensured.[10]

In the past, postmortem research was conducted to study the dissolution behavior of solid oxides in slags. In these studies, shaped oxide material (e.g., disks, cylinders) was dipped statically or was rotated in liquid slag for a fixed time.[11–14] This method is quite cumbersome and requires many numbers of samples to obtain a dissolution rate. High-temperature confocal scanning laser microscopy (HT-CSLM) enables *in situ* dissolution studies of oxide particles (e.g., nonmetallic inclusions) in slags at high temperatures relevant to steelmaking processes. Previous HT-CSLM studies mainly focused on the dissolution of Al_2O_3, MgO, and $MgAl_2O_4$, in $CaO–Al_2O_3–SiO_2$ or $CaO–Al_2O_3–SiO_2–MgO$ slags. However, irregular shape of the particles generated rotation during the dissolution, which was reported as a main source for experimental scatter and uncertainties about the governing reaction mechanism.

For the interpretation of the dissolution mechanism, the shrinking core model (SCM), which can be solved analytically, has been widely applied.[15–19] This model assumes one of two rate-controlling steps of the dissolution, namely chemical reaction at the interface between inclusion and slag, or mass transport of the dissolving species in the boundary layer of the slag. Later, a diffusion equation coupled with a lattice-Boltzmann modeling has been proposed to determine the underlying dissolution mechanism of Al_2O_3.[20–25] Although the latter approach is more versatile to elucidate the dissolution mechanism, it requires a high computational effort that is less attractive to be practically applied.[20]

As the HT-CSLM inclusion dissolution studies are a relatively new approach, only a few previous investigations are accessible. At present, to the best knowledge of the authors, no *in situ* study of the dissolution of SiO_2 in liquid slags remains known. Samaddar *et al.* conducted postmortem studies concerning the corrosion behavior of dipped polycrystalline alumina, single-crystalline sapphire, mullite, anorthite, and vitreous SiO_2 in a 40% CaO–20% Al_2O_3–40%

C. Jantzen—contributing editor

Manuscript No. 33314. Received June 4, 2013; approved September 19, 2013.
Based in part on the thesis submitted by Stefan Feichtinger for the M.S. degree in metallurgy, Montanuniversitaet Leoben, Austria, 2013.
[†]Author to whom correspondence should be addressed. e-mail: ybkang@postech.ac.kr

SiO_2 slag at temperatures between 1350°C and 1500°C. It was found that the dissolution of vitreous SiO_2 was controlled by diffusion in the boundary layer.[12]

In this study, to investigate the dissolution mechanism of SiO_2 inclusions in liquid slags, the HT-CSLM was employed using well-shaped spherical glassy SiO_2 particles. Slags with various compositions were tested to represent slags relevant to the steelmaking process of steel wire products. To avoid any solid layer on the SiO_2 particle, the slag composition was carefully determined by checking the $CaO–Al_2O_3–SiO_2$ phase diagram. Moreover, the use of a spherical particle ensures better accuracy for the measurement of the particle size during its dissolution, contrary to the use of irregular shaped particles in previous studies.[15–19] These two facts distinguish the present investigation from previous studies, and allowed a more reliable interpretation about the particle dissolution mechanism in fluids, such as inclusion dissolution in slags. It will be shown in this article that the dissolution pattern of the SiO_2 particle is strongly affected by the slag viscosity (relevant to mass transport), not by the concentration/activity of SiO_2 (relevant to chemical reaction). A modification in an existing model based on diffusion of SiO_2 in the slag is proposed to interpret the conducted SiO_2 dissolution experiments in this study.

II. Experimental Procedure

(1) High-temperature Confocal Scanning Laser Microscopy experiments

Details about HT-CSLM have been widely published.[26–30] After pioneering investigations by Emi *et al.*,[29,30] it has been identified that the advantages of using the HT-CSLM compared with a conventional optical microscope are twofold. The contrast of an image is significantly increased by using a laser as the light source, characterized by wavelengths below the thermal radiation spectrum of the observed samples. Because of a high maximum power of 1500 W of the heat source (a halogen lamp) and a low sample weight, high heating and cooling rates exceeding 1000°C/min are achievable. The maximum operating temperature is only limited by the chosen thermocouple and is about 1700°C at standard configuration.[27]

Six different slag samples were investigated in this study and the composition of each slag is listed in Table I. The experiments with slags 1–4 were carried out at the Chair of Ferrous Metallurgy, Montanuniversitaet Leoben, Austria. Experiments with slags 5 and 6 were conducted at the Graduate Institute of Ferrous Technology, Pohang University of Science and Technology (POSTECH), Republic of Korea. The experimental procedure on both microscopes was the same except for a minor difference [the refractory disk underneath the platinum crucible (Leoben: MgO, POSTECH: Al_2O_3)]. The two microscopes were of the same type (Lasertec, VL2000DX-SVF17SP, Yokohama, Japan). The temperature measurement of the sample in the platinum crucible was calibrated on both microscopes as described in Section II*(2)*.

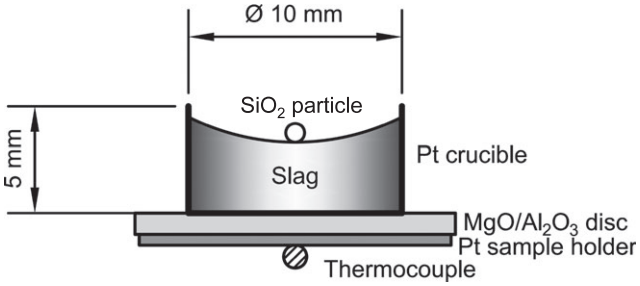

Fig. 1. Experimental setup employed in this study.

(A) Slag Preparation: The slags were prepared by mixing SiO_2, Al_2O_3, and $CaCO_3$ powders and premelting the mixture in platinum crucibles in an electrical heating furnace at 1600°C for 2 h. The liquid slags were then quenched on a stainless steel plate floating on water to prevent the slags from segregations and crystallizations. Subsequently, the glassy solid slag was crushed in an agate mortar. The chemical composition of the slag was then analyzed by X-ray fluorescence spectroscopy (XRF). For the dissolution experiments, the crushed slag powder was filled and compacted into the platinum crucibles (10 mm OD × 5 mm height). Then it was molten in an electrical furnace to avoid any foaming of the slag in the CSLM furnace. The premolten slag in the platinum crucible was then molten again in the CSLM furnace and cooled down rapidly by turning off the power of the CSLM furnace to prepare a homogeneous solidified chunk of slag on which a single SiO_2 particle was put for each experiment. The high cooling rates avoid segregations and crystallization during cooling. An MgO or Al_2O_3 disk was placed between the platinum crucible and the platinum sample holder to avoid sticking (Fig. 1). The slag compositions were chosen based on thermodynamic calculations which will be mentioned in Section II*(2)*.

(B) Thermocouple Calibration: To calibrate the thermocouples used in the HT-CSLM, two holes for the thermocouple wires (type R) were drilled into the cover glass of the HT-CSLM heating chamber. Subsequently, the thermocouple wires were stuck through the two holes and dipped into ground slag powder in the same platinum crucible which was also used for the experiments. The assembly was then heated up to the temperature range of interest (1000°C–1500°C). The temperature difference between the thermocouple dipped into the slag (TC-A) and the thermocouple beneath the sample holder of the HT-CSLM (TC-B) was logged every 50°C

Table I. Experimental Conditions, Physicochemical Properties of the Slags, and Results Obtained in this Study: (a) Slag Compositions, (b) Viscosity (η), (c) Activity of SiO_2 (with Respect to Pure Tridymite) of each Slag Sample, (d) (wt% SiO_2) in the Slag if the Slag Sample is Saturated by Solid SiO_2, (e) Experimentally Determined Average Dissolution Rate, (f) Dimensionless Saturation Concentration of each Slag Defined in Eq. (4), (g) Mean Diameter of SiO_2 Particles at the Beginning of Dissolution, and (h) Mean Dissolution Time of the Particle for each Slag. Slag Samples are Listed in the Order of Decreasing Viscosity of the Slags. Values in (b), (c), and (d) were Calculated at 1450°C by FactSage[34–36]

	(a)			(b)	(c)	(d)	(e)	(f)	(g)	(h)
	SiO_2	CaO	Al_2O_3							
Sample no.		(wt%)		η (Pa.s)	a_{SiO_2}	$(wt\% SiO_2)_{sat}$	Dissolution rate (μm/s)	k	Mean d_0 (μm)	Mean t_{total} (s)
Slag 1	54.6	34.1	10.6	2.41	0.46	67.6	1.45 ± 0.02	0.94	342 ± 3.4	235
Slag 2	50.5	38.3	10.6	1.25	0.31	67.3	3.18 ± 0.34	1.19	348 ± 17.8	110
Slag 5	37.1	36.4	26.5	1.08	0.09	70.5	3.63 ± 0.09	3.03	344 ± 1.7	95
Slag 6	42.3	38.8	18.9	1.02	0.14	69.1	3.84 ± 0.05	2.17	326 ± 2.2	85
Slag 3	45.3	43.7	10.4	0.60	0.16	66.9	8.51 ± 0.56	1.48	306 ± 5.5	36
Slag 4	42.8	46.6	10.8	0.47	0.10	66.8	11.02 ± 1.86	1.64	347 ± 29.9	34

after the furnace had reached a constant temperature. This temperature difference was then used to calibrate the temperature measured by TC-B which was used to set the experimental temperature.

(C) Dissolution Experiments: Each experiment was conducted by placing a single SiO_2 particle (diameter: ~350 μm) on the surface of the premolten slag in a platinum crucible as described in Section II*(1)* and heating up the assembly to the target temperature in the HT-CSLM. High-purity argon (flow rate of 100 cm^3/min) ensured a neutral atmosphere in the infrared furnace chamber. As the particle weight was less than 0.01% of the slag weight, composition changes by the dissolution of the particle were assumed to be negligible.

The polished spherical particles (Sandoz Fils, Cugy, Switzerland; ~350 μm) were made of commercially available vitreous high-purity (99.99%) SiO_2. The softening point is at 1650°C which means that the material exhibits a logarithmic viscosity of 6.6 Pa·s at this temperature.[31]

Figure 2 shows a typical heating cycle of the dissolution experiments. The scales are based on approximate values. The high heating rate of 1000°C/min ensured that the inclusion hardly started to dissolve before the experimental temperature was reached. At a temperature 50°C below the final temperature, the heating rate was reduced to 100°C/min to avoid overshooting.

The video saved by the HT-CSLM was converted into pictures by using the public domain software VirtualDub.[32] The pictures were then analyzed by the public domain image analysis software ImageJ.[33] A border was manually drawn around the dissolving particle. Under the assumption that the particle retains its spherical shape throughout the dissolution, an equivalent particle diameter was calculated from the measured inclusion area. Time zero in the interpretations was defined as the time when the experimental temperature had been reached. In this article, plots of the decreasing diameter versus time or normalized diameter (transient diameter divided by initial diameter) versus normalized time (time divided by total dissolution time) serve to elucidate the dissolution mechanism. For each slag, the same experiments were repeated three times to confirm reproducibility.

(2) Thermodynamic Calculations

The slag compositions used in this study were chosen to be both relevant to wire steel production and well suited to identify the role of the concentration/activity of SiO_2 and the slag viscosity on the dissolution of SiO_2 particles. The activity of SiO_2 in the slags with respect to pure tridymite was calculated using FactSage thermochemical computing system (ThermFact Ltd., Montreal, Canada and GTT-Technologies, Aachen, Germany) along with model parameters optimized by Bale *et al.* and Eriksson and Pelton.[34,35] The viscosity of the slag was also calculated by FactSage along with the viscosity model developed by Grundy *et al.*[36] The calculated results are shown in Table I.

Figure 3 shows a calculated isothermal section of the $CaO–SiO_2–Al_2O_3$ system at 1450°C by FactSage. Symbols shown in the figure correspond to the slag composition listed in Table I. Dotted lines and dashed lines are calculated iso-a_{SiO_2} and iso-viscosity lines, respectively (by FactSage as described above). Under the assumption of a straight dissolution path, it becomes clear that product layers will not form on the surface of the SiO_2 particle dissolving into the slag. This was also confirmed by a SEM/EDS micro analysis of a SiO_2 particle dissolving into the slag as shown in Fig. 4.

The compositions of the slags used in this study were designed with the aid of the thermodynamic analysis as follows: Slags 1–4 exhibit the same alumina content, but different SiO_2 concentrations. Slag 5 and slag 6 both show similar viscosities to slag 2. Slag 5 is characterized by a similar SiO_2 activity as slag 4, slag 6 has a similar SiO_2 activity as slag 3. The experimental temperature of 1450°C was chosen because of two reasons. On the one hand, the liquid slag phase field at this temperature is wide enough to allow for

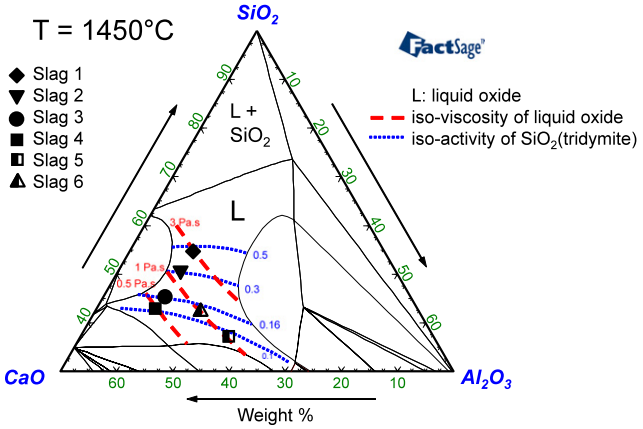

Fig. 3. Phase diagram of the $CaO–SiO_2–Al_2O_3$ system at 1450°C calculated by FactSage[34,35] showing the studied slag compositions (symbols), isoviscosity (dashed lines) and isoactivity lines (dotted lines).

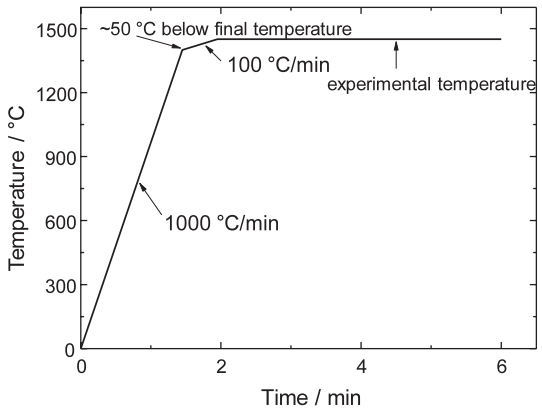

Fig. 2. Temperature profile for experiments with the SiO_2 particle in liquid slags with approximate axes scales.

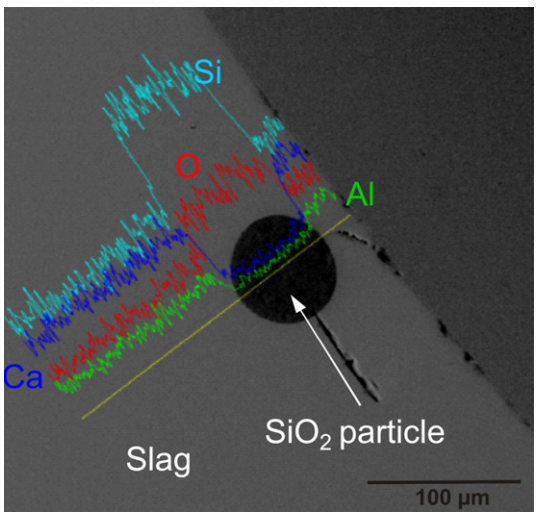

Fig. 4. Micrograph of a SiO_2 spherical particle dissolving into a slag composed of $CaO–SiO_2–Al_2O_3$ at 1450°C and a SEM-EDS line scan showing a qualitative comparison between the contents of Si, O, Ca, and Al.

the variation in the slag compositions. On the other hand, the inclusion dissolution rates are slow enough to obtain reproducible results and to distinguish between the dissolution times of slags with similar chemical compositions.

III. Results and Discussion

(1) Comparison of Dissolution Rates

Comprehensive interpretation of the dissolution mechanism requires the evaluation of the influence of slag properties on both the dissolution pattern and dissolution time. In this article, it will be discussed how the activity of SiO_2 in the slag and the slag viscosity affect the dissolution pattern.

The dissolution rates of SiO_2 inclusions in the slags at 1450°C are shown in Table I. The average dissolution rates were calculated by dividing the initial diameter by the total dissolution time. The slags are ordered by the dissolution rate. It is readily seen that there is a correlation between viscosity and average dissolution rate in such a way that an increasing viscosity decreases the dissolution rate. This agrees with the Eyring relation revealing that the diffusion coefficient is inversely proportional to the viscosity.[37] Moreover, the thickness of the boundary layer around the particle increases with increasing viscosity, resulting in a gentle concentration gradient.[38] If the dissolution is controlled by mass transfer (diffusion) in the boundary layer, a slag with higher viscosity would therefore lead to a slower dissolution.[12,37–40]

The second parameter which was considered is the activity of SiO_2 in the slag. The higher the activity of SiO_2, the closer is the slag to the SiO_2 saturation limit. In general, this means that slags with higher SiO_2 activities can be expected to dissolve SiO_2 inclusions more slowly than slags exhibiting low SiO_2 activities.[40,41]

Slag 5, slag 6, and slag 2 are characterized by similar viscosities. The SiO_2 activities of slag 5 and slag 4 as well as the SiO_2 activities of slag 6 and slag 3 are comparable. The dissolution rates of SiO_2 in slags 2, 5, and 6 are close to each other. However, the dissolution rate in slag 5 is significantly different to that in slag 4, and that in slag 6 is also much lower compared with slag 3. The results show that the influence of the viscosity might outweigh the influence of the SiO_2 activity in the slags investigated in this study.

Figures 5 and 6 show the dissolution patterns of SiO_2 particles in slag 1 and slag 3, respectively, represented by the measured particle diameter d versus the dissolution time t. Initial particle diameters for slag 3 in Fig. 6 were generally less than those for slag 1, which might be attributed to the faster dissolution of the particle in slag 3 before the final temperature in the HT-CSLM was reached. However, two experiments for slag 4 did not show such a faster dissolution at the beginning of the experiments. Therefore, the faster dissolution observed for slag 3 might occur due to local inhomogeneities of slag composition or slag temperature near the SiO_2 particle during the experiment. The average dissolution time in slag 1 was 235 s for a mean initial diameter of 342 μm. In slag 3, the average dissolution time was 36 s for an average initial inclusion diameter of 306 μm.

Figure 7 gives a comprehensive overview on the experimental results obtained in this study showing the normalized dissolution patterns of SiO_2 particles in all studied slags. As illustrated in the figure very clearly, increasing slag viscosity results in a transition of the SiO_2 particle dissolution pattern from a parabolic-like shape to an S-type shape, regardless of the activity of SiO_2.

(2) Common Kinetic Models

In previous investigations on oxide particle dissolution in various slags, the SCM has been widely applied to identify the rate controlling mechanism of the dissolution.[15–19] Levenspiel introduced a model which distinguishes between two

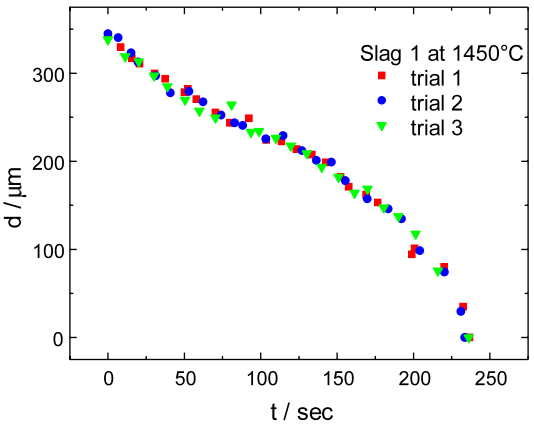

Fig. 5. Evolution of the SiO_2 particle diameter in slag 1 at 1450°C.

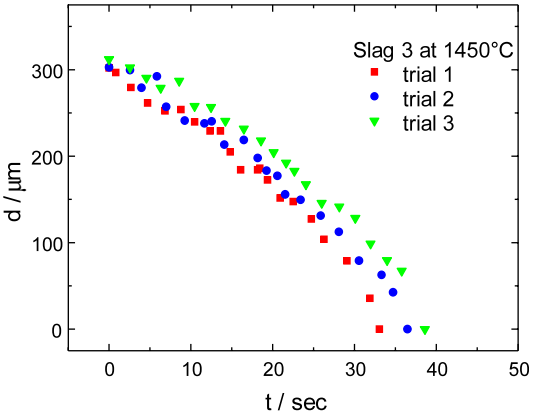

Fig. 6. Evolution of the SiO_2 particle diameter in slag 3 at 1450°C.

rate controlling steps, mass transfer (diffusion) control in a boundary layer (in a Stokes flow regime) and reaction rate control. Generally, it is presumed that the slag is saturated with the dissolving species at the interface between the slag and the dissolving particle.[40] The saturation or equilibrium concentration of the dissolving species is obtained by available phase diagrams or by thermodynamic calculations, under the assumption of a straight dissolution path.[15–17,19,25] A detailed explanation of the SCM can be found elsewhere.[40] Typical results proposed by the SCM are either a linear dependence of the particle size on the dissolution time in the case of reaction rate control, or a parabolic dependence of the particle size on the dissolution time in the case of mass transfer control.

In some cases the experimental results could not be described sufficiently by the SCM.[10,25] Alternatively, the solution of the diffusion equation may yield better results (diffusion into a stagnant fluid).[21,22,25] The diameter versus time curves show a typical S-shape when diffusion into a stagnant fluid is rate controlling. At the beginning of the dissolution, the steep concentration gradient around the particle leads to a fast dissolution rate. As the dissolution proceeds, the concentration gradient becomes less steep, thereby the dissolution rate decreases. Toward the end, the dissolution rate increases again as the volume of the particle becomes very small relative to the surface of the particle through which the dissolution occurs.[42] The diffusion equation for the dissolution of a spherical particle has to be solved numerically, contrary to the SCM which provides simple analytical solutions. Lattice Boltzmann modeling was proved to be a well suited method for the numerical treatment.[20–25]

Approximations of the diffusion equation for spherical inclusions can be used for analyzing if the dissolution is

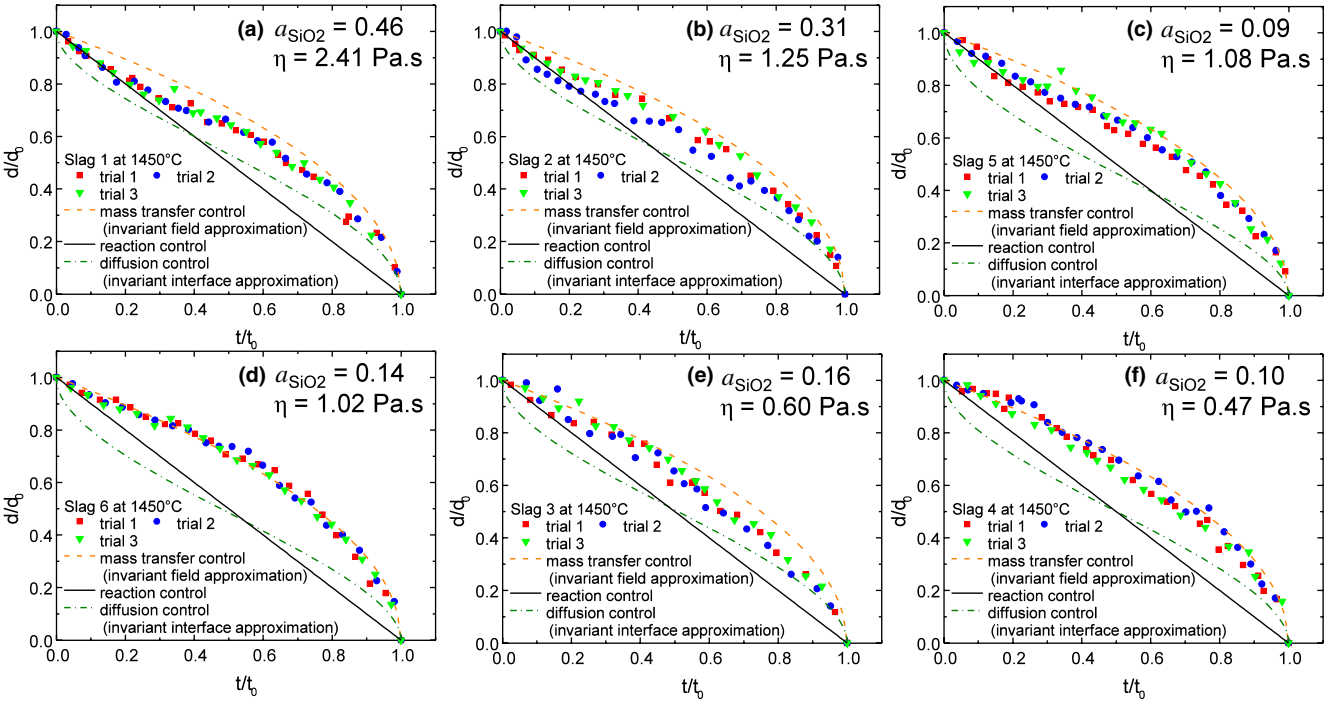

Fig. 7. Normalized dissolution patterns of SiO_2 particles in all the slags investigated in this study, in the order of decreasing viscosity of the slags.

governed by diffusion.[41,43,44] Dissolution controlled by diffusion in a stagnant fluid can generally be described by Fick's first and second laws of diffusion.[41,43,44] The stationary interface or invariant interface approximation assumes that the diffusion field is not altered by the movement of the interface between particle and slag. That means that the diffusion field would have stayed as if the particle/slag interface had been fixed at R_0 from the beginning of the dissolution (Fig. 8).[41,43,44] The concentration gradient of the dissolving species in the slag at the interface ($r = R$) between the particle and the slag is the driving force for the diffusion. For the case of dissolving particles in slags, the flux of solute from the interface equals the rate of loss of solute from the particle by the diffusion[41]:

$$-(c_p - c_{sat}) \cdot \frac{dR}{dt} = -D \cdot \left(\frac{\partial \Delta c}{\partial r}\right)_{r=R} \quad (1)$$

where r is the distance from the center of the particle, R is the radius of the particle, c_p, c_{sat}, and Δc are the concentrations of SiO_2 of the particle, that of the slag at the interface, and the difference of the SiO_2 concentrations at r and in the bulk slag (c_0) at a time t, respectively. D is an effective binary diffusion coefficient of SiO_2 in the slag.

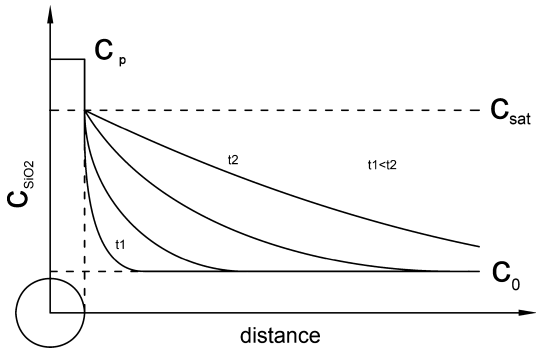

Fig. 8. A schematic concentration profile of the stationary interface/invariant size approximation.

Also, by Fick's second law of diffusion, the following equation is obtained:

$$\Delta c(r,t) = \frac{(c_{sat} - c_0) \cdot R}{r} \cdot erfc\left(\frac{r - R}{2 \cdot \sqrt{D \cdot t}}\right) \quad (2)$$

Combining Eqs. (1) and (2) yields the stationary interface or invariant interface approximation that has to be solved numerically[41]:

$$\frac{dR}{dt} = -\frac{k \cdot D}{R} - k \cdot \sqrt{\frac{D}{\pi \cdot t}} \quad (3)$$

The dimensionless saturation is defined as follows[41]:

$$k = \frac{c_{sat} - c_0}{c_p - c_{sat}} \quad (4)$$

The SiO_2 concentration c in the dimension kg/m^3 is obtained as follows:

$$c = x \cdot \rho \quad (5)$$

where x is a mass fraction of SiO_2 in the slag, and ρ is the slag density in kg/m^3.

On the other hand, the invariant field approximation is obtained by also neglecting the time-dependent change in the concentration profile in the slag. In other words, from the beginning of the dissolution on, the concentration profile has the same shape as for long times (steady state), as shown in Fig. 9[41,43,44]:

$$\frac{dR}{dt} = -\frac{k \cdot D}{R} \quad (6)$$

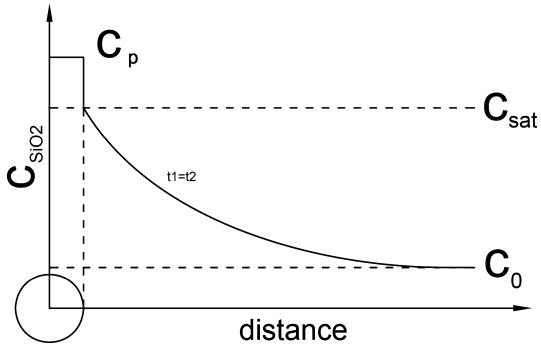

Fig. 9. A schematic concentration profile of the invariant field approximation.

when the equation above is used to derive the normalized dissolution curve (normalized radius versus normalized time), the same expression as in the mass transfer controlled SCM is obtained (a parabolic normalized dissolution curve).

Figure 10 shows the dissolution patterns measured in this study for the slags with the highest (slag 1) and the lowest viscosity (slag 4). d_0 is the initial diameter of the SiO_2 particle, t_{total} stands for the total dissolution time. Each symbol in the figure represents a fifth-order polynomial fit to the present authors' data of three experiments per each slag at 1450°C (R^2 of the fit is better than 0.99). Using the polynomial fits to the raw experimental data rather than using the raw data was considered to be helpful to show the two dissolution patterns for slag 1 and slag 4 distinctively. The S-shaped curve of slag 1 is similar to the curve of the invariant interface diffusion approximation. It has to be noted that the curve of the invariant interface diffusion approximation is affected by the dimensionless concentration k defined in Eq. (4) which depends on the slag composition c_0. In the figure, only one curve of the invariant interface diffusion approximation for $k = 1$ is shown for the sake of clarity.

The dissolution pattern of slag 4 shows parabolic-like shape similar to the curve of the mass transfer controlled SCM or the invariant field diffusion approximation. Nevertheless, it is not in perfect agreement with the proposed curve. The dissolution mechanisms of the different slags seem to depend on the viscosity of the slag. A transition of the pattern from an S-shaped curve for high viscosity slags (slag 1) to a parabolic-like curve for low viscosity slags (slag 4) was observed, which has never been identified in the previous investigations.[10,15–18,25] The normalized curves by those three different models in Fig. 10 show that the mentioned mathematical models cannot describe the experimental results sufficiently. The polynomial fits of the experimental results lie between the three calculated curves. It is thought that those models do not consider the role of the slag viscosity that has been identified to affect the dissolution mechanism. The transition from an S-shaped to a parabolic-like dissolution pattern could not be explained by the previously mentioned models. Even though real dimensionless concentration values k for slags 1 and 4, which can be easily calculated using the values given in Table I, were used for the calculation of the invariant interface diffusion approximation, it was not successful. It is likely that the dissolution in the six investigated slags is controlled by a mixture of boundary layer mass transfer and diffusion in the stagnant fluid of the slag. As the reaction rate controlled SCM does not seem to match the experimental results, it was excluded in the following considerations.

(3) Modification in the Previous Model

In this study, it is proposed to use a modified model based on approximations of the diffusion equation[41,43,44] that can be solved with less numerical effort. The concept of the modified mathematical model can be described by merging the two (invariant interface approximation and invariant field approximation) cases. When a slag exhibits high viscosity such as slag 1 in this study, the SiO_2 particle feels a resistance against moving in the slag. If the slag is extremely viscous, the particle is trapped in the slag, and the particle dissolution is only governed by diffusion in the stagnant fluid (slag) with virtually no boundary layer (or infinite boundary layer). Then, the dissolution of the particle should be described by the invariant size approximation. On the other hand, when the slag exhibits low viscosity similar to slag 4 in this study, the SiO_2 particle easily moves in the slag. If the slag is extremely fluid, the particle moves in the slag without resistance, and the dissolution of the particle is only governed by diffusion in the very thin boundary layer. In the actual case, due to finite viscosity of a slag, the particle moves in the slag with a finite resistance along with a boundary layer of finite thickness. This is now examined in more detail.

(A) When a Slag Exhibits High Viscosity (Fig. 11): Because of less convective flow, the concentration profile is

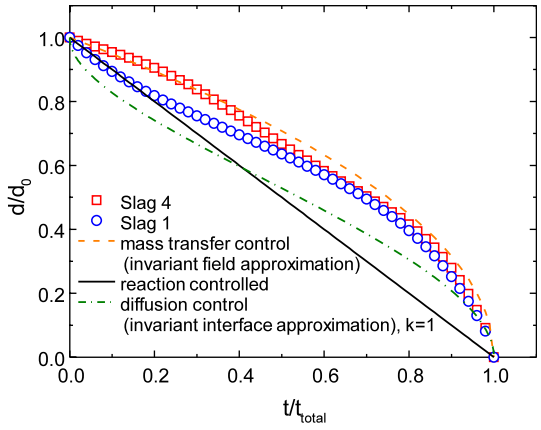

Fig. 10. Normalized dissolution pattern of SiO_2 inclusions in slag 1 and slag 4 at 1450°C. Symbols represent the present experimental data fitted to a fifth-order polynomial fit. Lines are calculated by several models: mass transfer controlled SCM or invariant field diffusion approximation (full line), reaction controlled SCM (dash-dot line), and diffusion in the stagnant fluid or stationary interface diffusion approximation (dashed line).

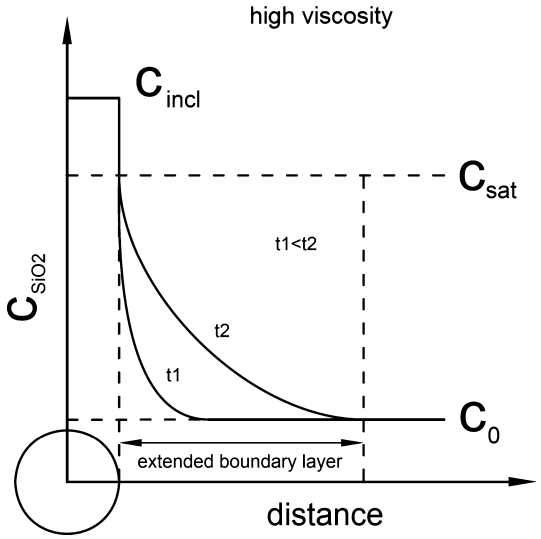

Fig. 11. Assumed concentration profile for inclusion dissolution in higher viscous slags.

not completely eliminated. It is assumed that a concentration profile evolves in an extended boundary layer surrounding the particle. At the beginning of the dissolution, the concentration gradient in the slag is steep and the dissolution is fast. As the concentration profile in the extended boundary layer evolves and the concentration gradient flattens out, the dissolution slows down. Nevertheless, particle movement and fluid flow prevent the concentration profile from being formed to a long distance which would result in an evident S-shaped dissolution curve. Consequently, in a slag with infinitely high viscosity without convective flow, particle movement and rotation, the dissolution would be governed by diffusion in a stagnant fluid only (S-shape). In the real case, however, the diffusion is effective only in the extended boundary layer, resulting in a less pronounced S-shaped dissolution curve.

(B) When a Slag Exhibits Low Viscosity (Fig. 12): In this case, a concentration profile is only formed in a thin boundary layer surrounding the particle as the particle can move rapidly in the slag. The concentration gradient in the boundary layer is almost unchanged throughout the dissolution, therefore the dissolution rate is mainly affected by the changing surface to volume ratio of the particle. For slags with infinitely low viscosity, it can be assumed that the dissolution pattern would be parabolic, governed by diffusion in the thin boundary layer. However, due to the finite viscosity of real slags, the concentration gradient in the boundary layer varies as the dissolution proceeds by building up SiO_2 around the particle. This results in a deviation from the parabolic curve which is only valid for the infinitely low viscosity case.

Therefore, a modification introduced in this study is based on the invariant interface or invariant size approximation of the diffusion equation [Eq. (3)].[41,43,44] The new modified model is obtained by introducing an additional factor f, to the second term of the Eq. (3):

$$\frac{dR}{dt} = -\frac{k \cdot D}{R} - f \cdot k \cdot \sqrt{\frac{D}{\pi \cdot t}} \tag{7}$$

The shape of the normalized dissolution curve is assumed to be affected by the slag viscosity as mentioned in the hypothesis above. For $f = 1$, which is the case for slags with infinitely high viscosity, the modified model turns into the invariant interface approximation. The normalized dissolution curve will then be evidently S-shaped. The shape of the curve also depends on the dimensionless saturation concentration k. For low saturation values and low resulting k values, the curve becomes less S-shaped, transforming toward a parabolic curve.

The second term in Eq. (3) stands for the time dependency of the concentration profile and is responsible for the fast dissolution at the beginning. With ongoing time, the second term becomes small and only the volume of the particle compared to the area of the diffusion zone is governing the dissolution rate.[42] For slags with infinitely low viscosity, the introduced factor f equals 0 and the modified mathematical model reduces to the invariant field approximation of Eq. (6) (parabolic normalized curve).[41,43,44]

Figure 13 shows calculated curves for the model test along with various f factors and values of k. The curve calculated with $f = 1$ shows evident S-shape which becomes more pronounced at higher k values (dimensionless saturation). The curves change toward a parabolic shape with decreasing f, as the time-dependent part of Eq. (7) has less impact.

(4) Model Calculations

Table I gives an overview of the slag properties at 1450°C which are relevant to the calculations. Also the mean initial diameter (d_0) and the mean total dissolution time (t_{total}) of the dissolution experiments are shown. The results stem from three experiments per slag with ~350 μm SiO_2 particles at 1450°C. The bulk slag concentrations c_0 were analyzed by XRF whereas the SiO_2 saturation concentrations c_{sat} were calculated by FactSage.[34,35] A collection of slag densities and density calculation models can be found in Slag Atlas.[37] The density of the bulk slag and the saturated slag are assumed to be equal due to a lack of reliable literature data for the studied slag compositions at 1450°C. The particle density can be found in data sheets of the manufacturer of the particles.[31]

To calculate the dissolution of the SiO_2 particles under the conditions employed in this study using the modified model, the dimensionless concentrations (k) in Eq. (7) were required. These values were calculated using Eq. (4). The parameter f was optimized to fit the experimental results for each slag with the modified model as exactly as possible. It can be regarded as a fitting parameter that is expected to be strongly related to the slag viscosity. The results can be summarized as follows.

Figure 14 shows the normalized dissolution pattern of slag 1. Slag 1 has the lowest dimensionless concentration k of all studied slags. The best fit with the modified model was obtained with a parameter f of 0.35.

The normalized results for slag 2 are pictured in Fig. 15. The experimental results exhibit a slight S-shape and more

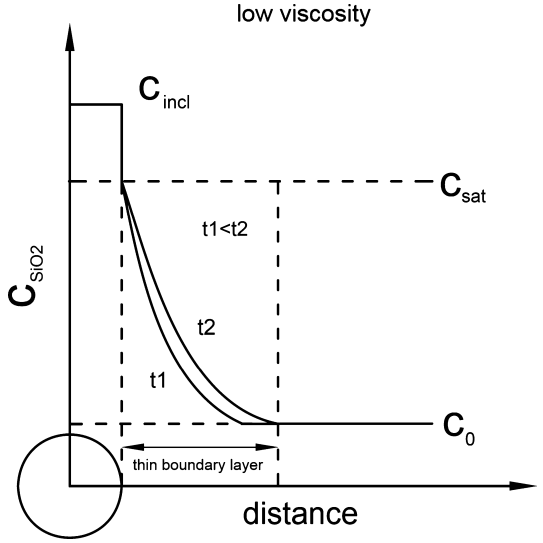

Fig. 12. Assumed concentration profile for inclusion dissolution in lower viscous slags.

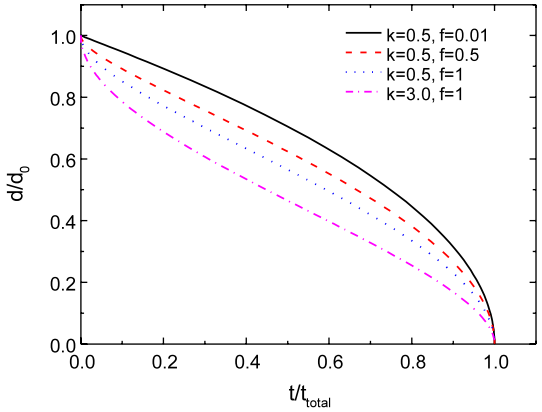

Fig. 13. Normalized dissolution curves for $k = 3$, and $k = 0.5$ with different f values calculated by the modified model.

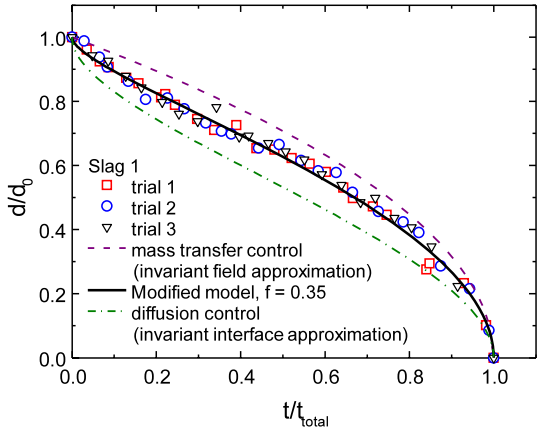

Fig. 14. Normalized dissolution behavior of SiO_2 inclusions in slag 1 compared with various mathematical models.

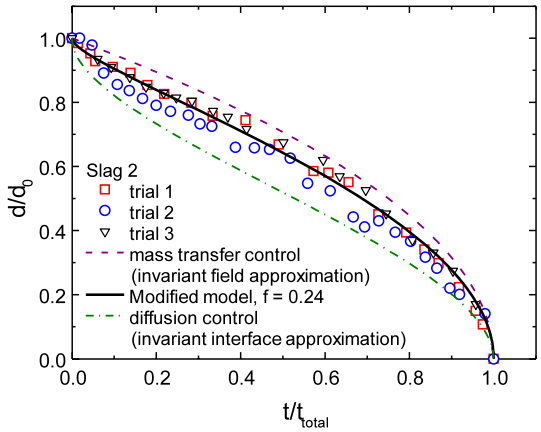

Fig. 15. Normalized dissolution behavior of SiO_2 inclusions in slag 2 compared with various mathematical models.

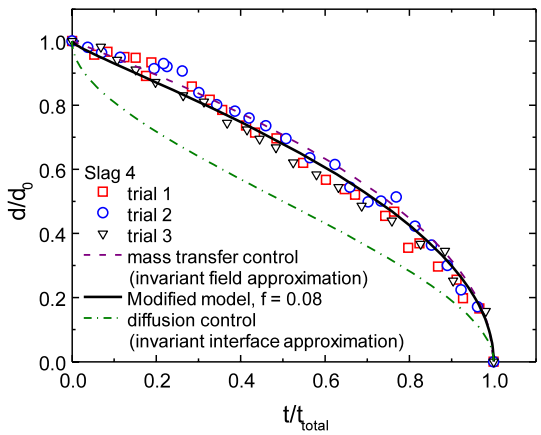

Fig. 16. Normalized dissolution behavior of SiO_2 inclusions in slag 4 compared with various mathematical models.

scatter than the results of slag 1. The modified model was found to be well suited with $f = 0.24$.

Slag 4 (Fig. 16) is characterized by the smallest fit parameter f (=0.08) of the four slags (slag 1 to slag 4) which reflects the parabolic-like shape of the pattern. Slag 1, slag 2, and slag 4 show that the shape of the normalized experimental results changes from S-shaped to parabolic, as the viscosity of the slag decreases.

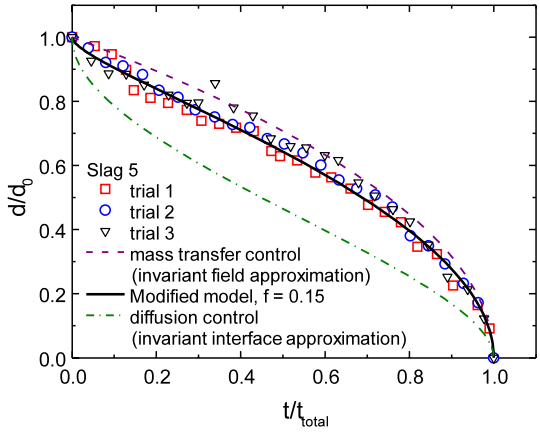

Fig. 17. Normalized dissolution behavior of SiO_2 inclusions in slag 5 compared with various mathematical models.

Table II. Fit Parameter f and Calculated Effective Binary Diffusion Coefficients for SiO_2 Dissolution at 1450°C

Sample no.	f	D (m²/s)
Slag 1	0.35	4.44×10^{-11}
Slag 2	0.24	8.49×10^{-11}
Slag 3	0.13	1.80×10^{-10}
Slag 4	0.08	2.38×10^{-10}
Slag 5	0.15	3.79×10^{-11}
Slag 6	0.10	6.03×10^{-11}

The normalized curve of slag 5 (Fig. 17) looks similar to the normalized results of slag 2. Both viscosity and f ($\eta = 1.08$, $f = 0.15$) of slag 5 are similar to those of slag 2 ($\eta = 1.25$, $f = 0.24$).

(5) More Utilization of the Model

After determining the parameters f by comparing the normalized results with the modified model, the effective binary diffusion coefficient D in the Eq. (7) can be obtained using the mean initial diameter and total dissolution time of each slag. Table II shows the parameters f and the calculated effective binary diffusion coefficients of the slags investigated in this study.

In Fig. 18, the parameter f versus slag viscosity is plotted for each slag. The modified model is based on the assumption that the normalized curve of particle dissolution in a slag with infinitely low viscosity should reduce to a parabolic shape. Consequently, a linear regression line should direct to the origin (zero viscosity and zero f) to reflect the physical background chosen in the modified model. The obtained correlation between the viscosity of slag and the fit parameter f is thus

$$f = 0.15006 \times \eta \tag{8}$$

where η is in Pa·s.

The regression equation enables the factor f to be estimated from a known slag viscosity, and consequently allows for the calculation of the dissolution curve along with the dimensionless concentration k.

Figure 19 shows the correlation between the calculated effective binary diffusion coefficients and the inverse of the slag viscosities. The calculated diffusion coefficients have to be seen as effective binary diffusion coefficients. That means that the system is reduced to a pseudobinary system consist-

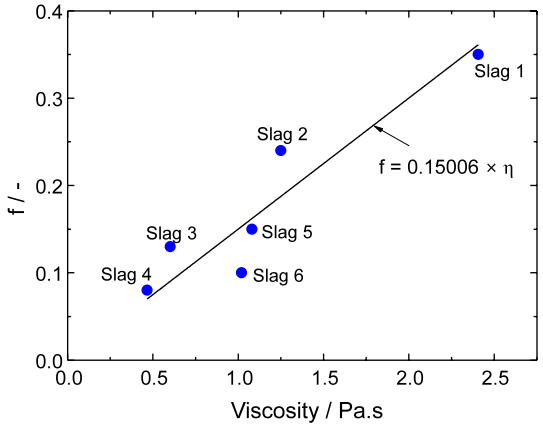

Fig. 18. Correlation between the fit parameter f and the slag viscosity at 1450°C.

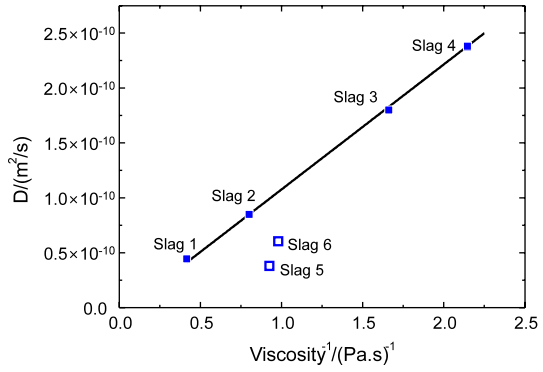

Fig. 19. Correlation between the calculated effective binary diffusion coefficients and the inverse of slag viscosities at 1450°C.

ing of the considered diffusing component and the slag consisting of the remaining components.[45] For slags 1–4, the correlation exhibits an almost clear linear relationship. Nevertheless, it can be seen that the effective binary diffusion coefficients of slags 5 and 6 deviate clearly from the linear relationship. It has to be noted that slags 1–4 contain 10.4–10.8 wt% Al_2O_3, whereas slags 5 and 6 contain 26.5 and 18.9 wt% Al_2O_3, respectively. At present, it is not clear how Al_2O_3 affects the diffusion coefficient. However, it is thought that one set of slags (1–4) and the other set of slags (5–6) are in different "effective" binary systems, thereby having different effective diffusion coefficient. This might be a reason for the lower effective binary diffusion coefficients in slags 5 and 6.

In an *ex situ* study of the dissolution of fused SiO_2, the governing mechanism was found to be boundary layer diffusion. A value of 4.5×10^{-12} m²/s was reported as the diffusion coefficient for SiO_2 in a 40% CaO–20% Al_2O_3–40% SiO_2 slag at 1425°C.[12] Majdic and Wagner determined the diffusion coefficient of SiO_2 in different slags at different temperatures. For a slag composed of 38.5% CaO–16.5% Al_2O_3–45% SiO_2, a SiO_2 diffusion coefficient of 2.8×10^{-10} m^2/s at 1500°C was found.[46] The chemical composition of slag 6 in this study is comparable with the two mentioned slags. For slag 6, the effective binary diffusion coefficient of SiO_2 at 1450°C was found to be 6.03×10^{-11} m^2/s which is in the range of the two reported values. It has to be noted though that *ex situ* studies with fixed refractories dipped into a stagnant fluid might be better suited if the purpose of the investigation is to obtain diffusion coefficients quantitatively.

IV. Conclusions

The dissolution behavior of well-shaped spherical SiO_2 particles in a number of CaO–Al_2O_3–SiO_2 slags at 1450°C was investigated using HT-CSLM. The dissolution mechanism was analyzed with the aid of thermodynamic calculations and the diffusion equation. By calculating the CaO–Al_2O_3–SiO_2 phase diagram, it was shown that reaction layers were not expected to form during the dissolution.

Slags with higher viscosities resulted in longer dissolution times. The correlation between SiO_2 activity and average inclusion dissolution rates did not show a meaningful agreement. Slags with higher viscosities tend to show a slightly S-shaped normalized dissolution pattern whereas slags with lower viscosity were characterized by a parabolic-like pattern. Such a transition of the dissolution pattern, which should reflect the reaction mechanism, could not be interpreted by the commonly used models.

Based on approximations of the diffusion equation, a modified model was proposed. It considers that the formation of the concentration profile in the slag depends on convective flow in the slag and particle movement which are both influenced by the slag viscosity. The results reveal a correlation between slag viscosity and the fit parameter f of the modified model. The calculated effective binary diffusion coefficients are in favorable agreement with literature data.

Acknowledgments

The authors thank Prof. Chong Soo Lee, Prof. Hae-Geon Lee, Mr. In-Hyeon Jeong, and other students of Graduate Institute of Ferrous Technology, POSTECH, for their support for staying and carrying out the experiments in Pohang, Republic of Korea. The contribution of Mr. Siegfried Schider through assisting the experiments and evaluations in Leoben, Austria is highly acknowledged. Financial support by the Austrian Federal Government (in particular from the Bundesministerium für Verkehr, Innovation und Technologie and the Bundesministerium für Wirtschaft, Familie und Jugend) and the Styrian Provincial Government, represented by Oesterreichische Forschungsfoerderungsgesellschaft mbH and by Steirische Wirtschaftsfoerderungsgesellschaft mbH, within the research activities of the K2 Competence Centre on "Integrated Research in Materials, Processing and Product Engineering", operated by the Materials Center Leoben Forschung GmbH in the framework of the Austrian COMET Competence Centre Programme, is gratefully acknowledged. One of the authors (YBK) also thanks POSCO Ltd. for the financial support through Steel Innovation Program.

References

[1]M. Yilmaz, "Failures During the Production and Usage of Steel Wires," *J. Mater. Process. Technol.*, **171** [2] 232–9 (2006).
[2]J. D. Seo, Y. T. Kim, and D. H. Kim, "Nonmetallic Inclusion Control of Steel for Tyrecord and saw Wire"; pp. 1–5 in 5th International Congress on the Science and Technology of Steelmaking, Dresden, Germany, 2012.
[3]S. K. Choudhary, "Influence of Modified Casting Practice on Steel Cleanliness," *ISIJ Int.*, **51** [4] 557–65 (2011).
[4]Y.-B. Kang and H.-G. Lee, "Inclusions Chemistry for Mn/Si Deoxidized Steels: Thermodynamic Predictions and Experimental Confirmations," *ISIJ Int.*, **44** [6] 1006–15 (2004).
[5]S. Nurmi, S. Louhenkilpi, and L. Holappa, "Optimization of Intensified Silicon Deoxidation," *Steel Res. Int.*, **84** [4] 323–7 (2013).
[6]S. K. Choudhary, S. Chandra, and A. Ghosh, "Prediction of Deoxidation and Inclusion Precipitation in Semikilled Steel," *Metall. Mater. Trans. B*, **36** [1] 59–66 (2005).
[7]H. Suito and R. Inoue, "Thermodynamics on Control of Inclusions Composition in Ultra-Clean Steels," *ISIJ Int.*, **36** [5] 528–36 (1996).
[8]H. Wang, F. Wang, Z. Xu, and L. Jin, "Composition Control of CaO–MgO–Al_2O_3–SiO_2 Inclusions in Tire Cord Steel – a Thermodynamic Analysis," *Steel Res. Int.*, **79** [1] 25–30 (2008).
[9]T. Ohshiro, T. Ikeda, H. Matsuyama, S. Okushima, Y. Oki, and N. Ibaraki, "Verbesserung der Dauerhaltbarkeit von Ventilfederdraht (Improvement of the Service Life of Valve Spring Wire)," *Stahl Eisen*, **109** [21] 1011–5 (1989).
[10]S. H. Lee, C. Tse, K. W. Yi, P. Misra, V. Chevrier, C. Orrling, S. Sridhar, and A. W. Cramb, "Separation and Dissolution of Al_2O_3 Inclusions at Slag/Metal Interfaces," *J. Non-Cryst. Solids*, **282** [1] 41–8 (2001).
[11]X. Yu, R. J. Pomfret, and K. S. Coley, "Dissolution of Alumina in Mold Fluxes," *Metall. Mater. Trans. B*, **28** [2] 275–9 (1997).
[12]B. N. Samaddar, W. D. Kingery, and A. R. Cooper, "Dissolution in Ceramic Systems: II, Dissolution of Alumina, Mullite, Anorthite, and Silica in a Calcium-Aluminum-Silicate Slag," *J. Am. Ceram. Soc.*, **47** [5] 249–54 (1964).

[13]A. Bui, H.-M. Ha, I. S. Chung, and H.-G. Lee, "Dissolution Kinetics of Alumina Into Mold Fluxes for Continuous Steel Casting," *ISIJ Int*., **45** [12] 1856–63 (2005).

[14]S. Taira, K. Nakashima, and K. Mori, "Kinetic Behavior of Dissolution of Sintered Alumina Into $CaO–SiO_2–Al_2O_3$ Slags," *ISIJ Int*., **33** [1] 116–23 (1993).

[15]J. Liu, M. Guo, P. T. Jones, F. Verhaeghe, B. Blanpain, and P. Wollants, "*In Situ* Observation of the Direct and Indirect Dissolution of MgO Particles in $CaO–Al_2O_3–SiO_2$-Based Slags," *J. Eur. Ceram. Soc*., **27** [4] 1961–72 (2007).

[16]B. J. Monaghan and L. Chen, "Dissolution Behavior of Alumina Micro-Particles in $CaO–SiO_2–Al_2O_3$ Liquid Oxide," *J. Non-Cryst. Solids*, **347** [1–3] 254–61 (2004).

[17]A. Fox, M. Valdez, J. Gisby, R. Atwood, P. Lee, and S. Sridhar, "Dissolution of ZrO_2, Al_2O_3, MgO and $MgAl_2O_4$ Particles in a B_2O_3 Containing Commercial Fluoride-Free Mould Slag," *ISIJ Int*., **44** [5] 836–45 (2004).

[18]S. Sridhar and A. W. Cramb, "Kinetics of Al_2O_3 Dissolution in $CaO–MgO–SiO_2–Al_2O_3$ Slags: *In Situ* Observations and Analysis," *Metall. Mater. Trans. B*, **31** [2] 406–10 (2000).

[19]B. J. Monaghan and L. Chen, "Effect of Changing Slag Composition on Spinel Inclusion Dissolution," *Ironmaking Steelmaking*, **33** [4] 323–30 (2006).

[20]F. Verhaeghe, B. Blanpain, and P. Wollants, "Dissolution of a Solid Sphere in a Multicomponent Liquid in a Cubic Enclosure," *Modell. Simul. Mater. Sci. Eng*., **16** [4] 045007 (2008).

[21]F. Verhaeghe, J. Liu, M. Guo, S. Arnout, B. Blanpain, and P. Wollants, "Determination of the Dissolution Mechanism of Al_2O_3 in $CaO–Al_2O_3–SiO_2$ Liquids Using a Combined Experimental-Numerical Approach," *J. Appl. Phys*., **103** [2] 023506, 8pp (2008).

[22]F. Verhaeghe, J. Liu, M. Guo, S. Arnout, B. Blanpain, and P. Wollants, "Dissolution and Diffusion Behavior of Al_2O_3 in a $CaO–Al_2O_3–SiO_2$ Liquid: An Experimental-Numerical Approach," *Appl. Phys. Lett*., **91** [12] 124104, 3pp (2007).

[23]F. Verhaeghe, S. Arnout, B. Blanpain, and P. Wollants, "Lattice Boltzmann Model for Diffusion-Controlled Dissolution of Solid Structures in Multicomponent Liquids," *Phys. Rev. E*, **72** [3] 036308, 4pp (2005).

[24]F. Verhaeghe, S. Arnout, B. Blanpain, and P. Wollants, "Lattice-Boltzmann Modeling of Dissolution Phenomena," *Phys. Rev. E*, **73** [3] 036316, 10pp (2006).

[25]J. Liu, F. Verhaeghe, M. Guo, B. Blanpain, and P. Wollants, "*In Situ* Observation of the Dissolution of Spherical Alumina Particles in $CaO–Al_2O_3–SiO_2$ Melts," *J. Am. Ceram. Soc*., **90** [12] 3818–24 (2007).

[26]C. Orrling, S. Sridhar, and A. W. Cramb, "*In Situ* Observation of the Role of Alumina Particles on the Crystallization Behavior of Slags," *ISIJ Int*., **40** [9] 877–85 (2000).

[27]C. Bernhard, S. Schider, A. Sormann, G. Xia, and S. Ilie, "Erste Ergebnisse des Neuen Hochtemperatur-Konfokalmikroskops am Lehrstuhl für Metallurgie (First Results of the High-Temperature Laser Scanning Confocal Microscope at the Montanuniversitaet Leoben)," *Berg- Huettenmaenn. Monatsh*., **156** [5] 161–7 (2011).

[28]P. T. Jones, D. Desmet, M. Guo, D. Durinck, F. Verhaeghe, J. van Dyck, J. Liu, B. Blanpain, and P. Wollants, "Using Confocal Scanning Laser Microscopy for the *In Situ* Study of High-Temperature Behaviour of Complex Ceramic Materials," *J. Eur. Ceram. Soc*., **27** [12] 3497–507 (2007).

[29]H. Chikama, H. Shibata, T. Emi, and M. Suzuki, ""*In Situ*" Real Time Observation of Planar to Cellular and Cellular to Dendritic Transition of Crystals Growing in Fe–C Alloy Melts," *Mater. Trans., JIM*, **37** [4] 620–6 (1996).

[30]H. Yin, T. Emi, and H. Shibata, "Determination of Free Energy of Delta-Ferrite/Gamma-Austenite Interphase Boundary of Low Carbon Steels by *In Situ* Observation," *ISIJ Int*., **38** [8] 794–801 (1998).

[31]Product Data Sheet, Available at: http://www.sandoz.ch/2002/products/characteristique/quartz.pdf

[32]VirtualDub, Version 1.9.10, developed by A. Lee. Available at: http://www.virtualdub.org

[33]ImageJ, Version 1.45s, developed at U.S. National Institutes of Health. Available at: http://imagej.nih.gov/ij/.

[34]C. W. Bale, E. Belisle, P. Chartrand, S. A. Degterov, G. Eriksson, K. Hack, I.-H. Jung, Y.-B. Kang, J. Melançon, A. D. Pelton, C. Robelin, and S. Petersen, "Factsage Thermochemical Software and Databases – Recent Developments," *Calphad*, **33** [2] 295–311 (2009).

[35]G. Eriksson and A. D. Pelton, "Critical Evaluation and Optimization of the Thermodynamic Properties and Phase Diagrams of the $CaO–Al_2O_3$, $Al_2O_3–SiO_2$, and $CaO–Al_2O_3–SiO_2$ Systems," *Metall. Trans. B*, **24B** [5] 807–16 (1993).

[36]A. N. Grundy, I.-H. Jung, A. D. Pelton, and S. A. Decterov, "A Model to Calculate the Viscosity of Silicate Melts: Part II: The $NaO_{0.5}–MgO–CaO–AlO_{1.5}–SiO_2$ System," *Int. J. Mater. Res*., **99** [11] 1195–209 (2008).

[37]K. C. Mills and B. J. Keene, *Slag Atlas* (Chapter 8 and 13). 2nd edition, Verein deutscher Eisenhuettenleute, Verlag Stahleisen, Duesseldorf, Germany, 1981.

[38]J. Ahrendts and S. Kabelac, *Huette. Das Ingenieurwissen*. (Engineering knowledge) (Chapter F), 33rd edition, Edited by H. Czichos and M. Hennecke. Springer, Berlin, Heidelberg, New York, 2007.

[39]A. R. Cooper and W. D. Kingery, "Dissolution in Ceramic Systems: I, Molecular Diffusion, Natural Convection, and Forced Convection Studies of Sapphire Dissolution in Calcium Aluminum Silicate," *J. Am. Ceram. Soc*., **47** [1] 37–43 (1964).

[40]O. Levenspiel, *Chemical Reaction Engineering*. (Chapter 25), 3rd edition, John Wiley & Sons, New York, 1999.

[41]M. J. Whelan, "On the Kinetics of Precipitate Dissolution," *Met. Sci. J*., **3** [1] 95–7 (1969).

[42]H. B. Aaron and G. R. Kotler, "Second Phase Dissolution," *Metall. Trans*., **2** [2] 393–408 (1971).

[43]H. B. Aaron, D. Fainstein, and G. R. Kotler, "Diffusion-Limited Phase Transformations – a Comparison and Critical Evaluation of Mathematical Approximations," *J. Appl. Phys*., **41** [11] 4404–10 (1970).

[44]L. C. Brown, "Diffusion-Controlled Dissolution of Planar, Cylindrical, and Spherical Precipitates," *J. Appl. Phys*., **47** [2] 449–58 (1976).

[45]Y. X. Zhang, "A Modified Effective Binary Diffusion Model," *J. Geophys. Res. [Solid Earth]*, **98** [B7] 11901–20 (1993).

[46]A. Majdic and H. Wagner, "Diffusion Von Silizium in Schmelzfluessigen Kalk-Kieselsaeure-Tonerde-Schlacken (Diffusion of Silicon in Molten Lime-Silica-Alumina Slags)," *Arch. Eisenhuettenwes*, **41** [6] 529–32 (1970). □